A Stochastic Optimization Approach for an Integrated Energy System with Electricity, Heat, Gas, and Hydrogen Considering Carbon Trading

Qiang Li [1], *Zhonghao* Wang[1], *Bo* Jiang[1], *Fuxiang* Dong[1], *Jinfu* Liu[1*], *Peigang* Yan[1] and *Daren* Yu[1,2]

[1]School of Energy Science and Engineering, Harbin Institute of Technology, 150001 Harbin, Heilongjiang, China
[2]School of Astronautics, Harbin Institute of Technology, 150001 Harbin, Heilongjiang, China

Abstract. Targeting low-carbon energy transition, this study proposes a stochastic optimization model for an integrated electricity-heat-gas-hydrogen system with high renewable penetration. The configuration couples four storage assets—battery, heat storage tank, gas storage tank and hydrogen storage tank—with three hydrogen devices: electrolyzers, fuel cells and methanation reactors. Operating and carbon-trading costs are both embedded. Numerical results indicate that enabling carbon trading mildly raises computational load yet increases operating cost while curbing renewable curtailment. Integrating hydrogen devices significantly heightens model complexity, further lowers curtailment and reduces overall cost, validating the practical value of the approach.

* Corresponding author: jfliuhit@163.com

© The Authors, published by EDP Sciences. This is an open access article distributed under the terms of the Creative Commons Attribution License 4.0 (https://creativecommons.org/licenses/by/4.0/).

1 Introduction

Driven by the dual-carbon targets of peaking and neutrality, power-system portfolios are being restructured through the accelerated retirement of coal-fired units. The concomitant large-scale integration of variable renewable generation intensifies the demand for operational flexibility [1-3]. Two broad strategies exist to narrow this gap: (i) installing additional storage, which incurs high capital costs and long lead times, or (ii) exploiting the intrinsic flexibility of integrated energy systems (IES) via multi-energy coupling, leveraging existing infrastructure.

Gas turbines emit fewer pollutants per unit of electricity than coal plants. Conventional IES coordinate electricity, heating/cooling, and natural-gas flows [4] ; yet natural-gas combustion still yields substantial CO_2, preventing deep decarbonization. Carbon-tax schemes now incentivize operators to retrofit IES by either integrating carbon capture and storage or substituting hydrogen for natural gas. Because carbon capture and storage remains capital-intensive and has long payback periods, near-term deployment is limited. Conversely, hydrogen integration can simultaneously cut CO_2 emissions and reduce operating expenditure. With a lower heating value roughly four times that of natural gas and near-zero end-use emissions, hydrogen is positioned to become a cornerstone of future IES.

Reference [5] formulates a multi-level heat-coupled IES model and aggregates the entire system into a single demand-response resource, but its scope is limited to thermal components. Reference [6] constructs a non-cooperative game among IES agents, operators, storage systems, and end-users, yet relies on a simplified network topology. Reference [7] presents a cross-regional, multi-storage coordination framework that pools distributed storage to simultaneously optimize economic, efficiency, and environmental objectives. Absent hydrogen technologies, such aggregation mechanisms already unlock flexibility and maximize system-wide revenue.

Recent work has embedded hydrogen technologies within IES frameworks. Targeting industrial-scale hydrogen loads, Reference [8] develops a real-time management framework that integrates hydrogen hubs, battery storage, renewables and gas units into a unified industrial integrated energy system, enabling online coordinated control of multiple resources. Reference [9] develops a hydrogen capacity-sizing method that jointly considers electricity–gas–heat demand response; numerical results show that combining hydrogen integration with demand response markedly reduces operating expenditure. Reference [10] proposes an IES fueled by hydrogen-enriched natural gas, achieving deep hydrogen–gas coupling that lowers costs and significantly reduces CO_2 emissions, thereby accelerating system decarbonization.

Current research on hydrogen-integrated energy systems exhibits two principal gaps. First, the coupling mechanisms between hydrogen devices and heterogeneous energy carriers remain insufficiently characterized. Second, uncertainties from stochastic renewable generation and diverse demand are largely neglected. To address these deficiencies, we propose a stochastic optimization model that (i) captures multiple uncertainties and (ii) co-optimizes the electricity–heat–gas–hydrogen nexus. The model simultaneously curtails carbon emissions and minimizes operational costs while enabling coordinated dispatch of all internal resources, thus accelerating the low-carbon transition of the energy sector.

The remainder of this paper is organized as follows. Section 2 describes the system architecture and formulates mathematical models for each resource. Section 3 presents the case-study parameters and data sources. Section 4 conducts numerical analyses and discussions. Section 5 concludes the study.

2 System description and model formulation

This section mainly completes the description of the IES, the objective function and constraints of the optimization problem.

2.1 System description

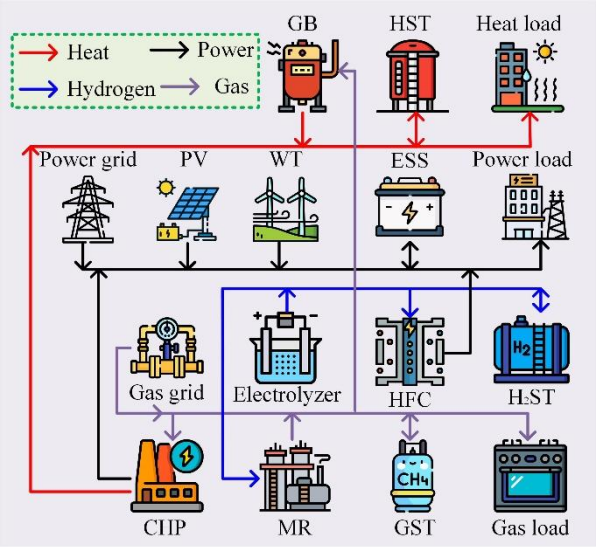

Fig. 1. The IES framework proposed in this study.

Fig. 1 depicts the IES architecture. This framework can be applied to small areas such as campuses and industrial zones, and specific equipment parameters can be modified based on actual equipment parameters. Four energy vectors—thermal, electrical, hydrogen, and natural gas—interact within the system. Thermal demand is supplied by combined heat and power (CHP) units, gas boilers (GB), and heat storage tanks (HST). Electrical demand is met by photovoltaic (PV) arrays, wind turbines (WT), an electrical storage system (ESS), CHP units, hydrogen fuel cells (HFC), and grid imports. Hydrogen balance is maintained by electrolyzers, HFC consumption, bidirectional hydrogen storage tanks (H_2ST), and methanation reactors (MR). Natural-gas demand is satisfied by CHP units, GB, MR, gas storage tanks (GST), and external supply.

2.2 Constraints

This section introduces the operational constraints and multiple balancing constraints of different resources within the system.

2.2.1 Renewable energy constraints

The IES incorporates PV and WT as renewable sources; their output constraints are:

$$0 \le p_{s,t}^{\mathrm{PV}} \le \overline{p}_{s,t}^{\mathrm{PV}} \tag{1}$$

$$0 \le p_{s,t}^{\mathrm{WT}} \le \overline{p}_{s,t}^{\mathrm{WT}} \tag{2}$$

where, $\overline{p}_{s,t}^{\mathrm{PV}}$ and $\overline{p}_{s,t}^{\mathrm{WT}}$ are the maximum output values of PV and WT respectively; $p_{s,t}^{\mathrm{PV}}$ and $p_{s,t}^{\mathrm{WT}}$ are the actual outputs of PV and WT after abandoning solar and wind respectively; $\overline{p}_{s,t}^{\mathrm{PV}} - p_{s,t}^{\mathrm{PV}}$ and $\overline{p}_{s,t}^{\mathrm{WT}} - p_{s,t}^{\mathrm{WT}}$ are the amount of abandoned solar power and abandoned wind respectively.

2.2.2 GB constraints

The GB is a natural-gas-fired unit producing thermal energy. Eq. (3) defines the gas-to-heat conversion efficiency; Eq. (4) sets the maximum gas intake; Eq. (5) enforces the ramp-rate limit.

$$h_{s,t}^{\mathrm{GB}} = \alpha_{\mathrm{e}}^{\mathrm{GB}} V_{s,t}^{\mathrm{GB,g}} \beta^{\mathrm{gas}} \tag{3}$$

$$\underline{V}^{\mathrm{CHP,g}} \le V_{s,t}^{\mathrm{GB,g}} \le \overline{V}^{\mathrm{CHP,g}} \tag{4}$$

$$-\Delta\overline{V}^{\mathrm{GB,g}} \le V_{s,t+1}^{\mathrm{GB,g}} - V_{s,t}^{\mathrm{GB,g}} \le \Delta\overline{V}^{\mathrm{GB,g}} \tag{5}$$

where, $\alpha_{\mathrm{e}}^{\mathrm{GB}}$ denotes the gas-to-heat efficiency of the GB; $V_{s,t}^{\mathrm{GB,g}}$ is the natural-gas consumption at time *t*; $h_{s,t}^{\mathrm{GB}}$ is the thermal power output at time *t*; $\overline{V}^{\mathrm{CHP,g}}$ and $\underline{V}^{\mathrm{CHP,g}}$ are the upper and lower limits of natural gas consumption by GB, respectively; $\Delta\overline{V}^{\mathrm{GB,g}}$ is the ramp-rate limit.

2.2.3 CHP constraints

The CHP unit combusts natural gas to generate electricity and recovers waste heat for thermal consumers. By optimizing its heat-to-power ratio, the unit meets both electricity and heat demand while minimizing fuel use. Operational constraints are given in Eqs. (3)–(7): Eq. (3) models electricity generation, Eq. (4) models waste-heat recovery, Eq. (5) limits natural-gas input, Eq. (6) sets the ramp-rate bound, and Eq. (7) restricts the heat-to-power ratio to its feasible range.

$$p_{s,t}^{\mathrm{CHP}} = \alpha_{\mathrm{e}}^{\mathrm{CHP}} V_{s,t}^{\mathrm{CHP,g}} \beta^{\mathrm{gas}} \tag{6}$$

$$h_{s,t}^{\mathrm{CHP}} = \alpha_{h}^{\mathrm{CHP}} V_{s,t}^{\mathrm{CHP,g}} \beta^{\mathrm{gas}} \tag{7}$$

$$\underline{V}^{\mathrm{CHP,g}} \le V_{s,t}^{\mathrm{CHP,g}} \le \overline{V}^{\mathrm{CHP,g}} \tag{8}$$

$$-\Delta\overline{V}^{\mathrm{CHP,g}} \le V_{s,t+1}^{\mathrm{CHP,g}} - V_{s,t}^{\mathrm{CHP,g}} \le \Delta\overline{V}^{\mathrm{CHP,g}} \tag{9}$$

$$\underline{\delta}^{\mathrm{CHP,g}} \le h_{s,t}^{\mathrm{CHP}} \Big/ p_{s,t}^{\mathrm{CHP}} \le \overline{\delta}^{\mathrm{CHP,g}} \tag{10}$$

where, where $\alpha_{\mathrm{e}}^{\mathrm{CHP}}$ denotes the gas-to-electricity efficiency of the CHP unit; $\alpha_{h}^{\mathrm{CHP}}$ is its gas-to-heat efficiency; β^{gas} the lower heating value of natural gas, kWh/m^3 ; $V_{s,t}^{\mathrm{CHP,g}}$ is the natural-gas consumption at time *t*, m^3 ; $p_{s,t}^{\mathrm{CHP}}$ and $h_{s,t}^{\mathrm{CHP}}$ the electrical and thermal power outputs at time *t*, kW ; $\overline{V}^{\mathrm{CHP,g}}$ and $\underline{V}^{\mathrm{CHP,g}}$ are the upper and lower bounds on natural-gas consumption , respectively; $\Delta\overline{V}^{\mathrm{CHP,g}}$ is the ramp-rate limit; $\overline{\delta}^{\mathrm{CHP,g}}$ and $\underline{\delta}^{\mathrm{CHP,g}}$ are the upper and lower bounds of the heat-to-power ratio , respectively.

2.2.4 Electrolyzer constraints

The electrolyzer splits water into hydrogen via an electrochemical reaction driven by electricity. Eq. (8) defines the electricity-to-hydrogen efficiency; Eq. (9) caps its power input; Eq. (10) enforces the ramp-rate limit.

$$V_{s,t}^{\mathrm{EL,H2}} = \alpha_{\mathrm{e}}^{\mathrm{EL}} p_{s,t}^{\mathrm{EL}} \Big/ \beta^{\mathrm{H_2}} \tag{11}$$

$$\underline{p}^{\mathrm{EL}} \le p_{s,t}^{\mathrm{EL}} \le \overline{p}^{\mathrm{EL}} \tag{12}$$

$$-\Delta\overline{p}^{\mathrm{EL}} \le p_{s,t+1}^{\mathrm{EL}} - p_{s,t}^{\mathrm{EL}} \le \Delta\overline{p}^{\mathrm{EL}} \tag{13}$$

where, $\alpha_{\mathrm{e}}^{\mathrm{EL}}$ is the electricity-to-hydrogen efficiency of the electrolyzer; $\beta^{\mathrm{H_2}}$ is the calorific value of hydrogen, kWh/m^3 ; $p_{s,t}^{\mathrm{EL}}$ is the power consumption of the electrolytic at time *t*, kW ; $\overline{p}^{\mathrm{EL}}$ and $\underline{p}^{\mathrm{EL}}$ are the upper and lower limits of the power consumption of the electrolyzer at time *t*, respectively; $\Delta\overline{p}^{\mathrm{EL}}$ is the upper limit of the climbing constraint of the electrolyzer.

2.2.5 MR constraints

The MR catalytically converts hydrogen and carbon dioxide into methane. Equation (11) defines the hydrogen-to-methane conversion efficiency; Eq. (12) caps the hydrogen feedstock flow; Eq. (13) enforces the ramp-rate limit.

$$V_{s,t}^{\mathrm{MR,gas}} = \alpha_{\mathrm{e}}^{\mathrm{MR}} V_{s,t}^{\mathrm{MR,H2}} \beta^{\mathrm{H2}} \Big/ \beta^{\mathrm{gas}} \tag{14}$$

$$\underline{V}^{\mathrm{MR,H_2}} \le V_{s,t}^{\mathrm{MR,H_2}} \le \overline{V}^{\mathrm{MR,H_2}} \tag{15}$$

$$-\Delta\overline{V}^{\mathrm{MR,H_2}} \le V_{s,t+1}^{\mathrm{MR,H_2}} - V_{s,t}^{\mathrm{MR,H_2}} \le \Delta\overline{V}^{\mathrm{MR,H_2}} \tag{16}$$

where, $\alpha_{\mathrm{e}}^{\mathrm{MR}}$ is the hydrogen-methane conversion efficiency of MR at time *t*; $V_{s,t}^{\mathrm{MR,H2}}$ is the volume of hydrogen consumed by MR at time *t*, m^3 ; $V_{s,t}^{\mathrm{MR,gas}}$ is the volume of methane generated by MR at time *t*, m^3 ; $\overline{V}^{\mathrm{MR,H_2}}$ and $\underline{V}^{\mathrm{MR,H_2}}$ are the upper and lower limits of hydrogen consumption by MR at time *t*, respectively; $\Delta\overline{V}^{\mathrm{MR,H_2}}$ is the upper limit of the ramp constraint of MR.

2.2.6 HFC constraints

The HFC converts hydrogen into electricity via an electrochemical reaction. Eq. (14) defines the hydrogen-to-electricity efficiency, Eq. (15) bounds hydrogen consumption, and Eq. (16) limits the ramp rate.

$$p_{s,t}^{\mathrm{HFC}} = \alpha_{\mathrm{e}}^{\mathrm{HFC}} V_{s,t}^{\mathrm{HFC,H_2}} \beta^{\mathrm{H_2}} \tag{17}$$

$$\underline{V}^{\mathrm{HFC,H_2}} \le V_{s,t}^{\mathrm{HFC,H_2}} \le \overline{V}^{\mathrm{HFC,H_2}} \tag{18}$$

$$-\Delta\overline{V}^{\mathrm{HFC,H_2}} \le V_{s,t+1}^{\mathrm{HFC,H_2}} - V_{s,t}^{\mathrm{HFC,H_2}} \le \Delta\overline{V}^{\mathrm{HFC,H_2}} \tag{19}$$

where, $\alpha_{\mathrm{e}}^{\mathrm{HFC}}$ is the hydrogen-to-electricity efficiency of the HFC; $V_{s,t}^{\mathrm{HFC,H_2}}$ is the volume of hydrogen consumed by the HFC at time t, m^3; $\overline{V}^{\mathrm{HFC,H_2}}$ and $\underline{V}^{\mathrm{HFC,H_2}}$ are the maximum and minimum values of hydrogen consumption of the HFC respectively; $\Delta\overline{V}^{\mathrm{HFC,H_2}}$ is the upper limit of the ramp constraint of the HFC.

2.2.7 Constraints of different energy storage devices

This study considers four storage types: ESS, HST, H_2ST, and GST. Because their operating constraints are structurally identical, only ESS is detailed; the others follow analogously. Eqs. (20)–(21) bound charge/discharge power, Eq. (22) governs the state-of-energy balance, Eq. (23) limits capacity, and Eq. (24) imposes identical initial and terminal energy levels over the scheduling horizon.

$$0 \le p_{s,t}^{\mathrm{ESS,c}} \le u_{s,t}^{\mathrm{ESS}} \overline{p}^{\mathrm{ESS,c}} \tag{20}$$

$$0 \le p_{s,t}^{\mathrm{ESS,d}} \le \left(1 - u_{s,t}^{\mathrm{ESS}}\right) \overline{p}^{\mathrm{ESS,d}} \tag{21}$$

$$\begin{aligned} S_{s,t+1}^{\mathrm{ESS}} = \; & S_{s,t}^{\mathrm{ESS}} + \alpha^{\mathrm{ESS,c}} p_{s,t}^{\mathrm{ESS,c}} \Delta t \\ & - \alpha^{\mathrm{ESS,d}} p_{s,t}^{\mathrm{ESS,d}} \Delta t \end{aligned} \tag{22}$$

$$\underline{S}^{\mathrm{ESS}} \le S_{s,t}^{\mathrm{ESS}} \le \overline{S}^{\mathrm{ESS}} \tag{23}$$

$$S_{s,1}^{\mathrm{ESS}} = S_{s,\mathrm{T}}^{\mathrm{ESS}} \tag{24}$$

where, $\alpha^{\mathrm{ESS,c}}$ and $\alpha^{\mathrm{ESS,d}}$ are the charging and discharging efficiencies of the ESS respectively; $\overline{p}^{\mathrm{ESS,c}}$ and $\overline{p}^{\mathrm{ESS,d}}$ are the charging and discharging of the ESS at time t respectively; $\overline{p}^{\mathrm{ESS,c}}$ and $\overline{p}^{\mathrm{ESS,d}}$ are the upper limits of charging and discharging of the ESS at time t respectively; $u_{s,t}^{\mathrm{ESS}}$ is a binary variable to ensure that the ESS is not charged or discharged at the same time; $S_{s,t}^{\mathrm{ESS}}$ is the capacity of ESS at time t; $\overline{S}^{\mathrm{ESS}}$ and $\underline{S}^{\mathrm{ESS}}$ are the upper and lower limits of the capacity of the ESS respectively.

2.2.8 Balance constraints

Eqs. (25)–(28) enforce the electrical, thermal, natural-gas, and hydrogen balance constraints, respectively. Eqs. (29) and (30) cap the power imported from the grid and the natural-gas purchased from the network.

$$\begin{aligned} & p_{s,t}^{\mathrm{PV}} + p_{s,t}^{\mathrm{WT}} + p_{s,t}^{\mathrm{CHP}} + p_{s,t}^{\mathrm{HFC}} + p_{s,t}^{\mathrm{buy}} \\ & + p_{s,t}^{\mathrm{ESS,d}} = p_{s,t}^{\mathrm{load}} + p_{s,t}^{\mathrm{EL}} + p_{s,t}^{\mathrm{ESS,c}} \end{aligned} \tag{25}$$

$$h_{s,t}^{\mathrm{GB}} + h_{s,t}^{\mathrm{CHP}} - h_{s,t}^{\mathrm{HST,c}} + h_{s,t}^{\mathrm{HST,d}} = h_{s,t}^{\mathrm{load}} \tag{26}$$

$$\begin{aligned} & V_{s,t}^{\mathrm{MR,gas}} + V_{s,t}^{\mathrm{GST,g,d}} + V_{s,t}^{\mathrm{buy,g}} = V_{s,t}^{\mathrm{GB,g}} \\ & + V_{s,t}^{\mathrm{CHP,g}} + V_{s,t}^{\mathrm{GST,g,c}} + V_{s,t}^{\mathrm{load,g}} \end{aligned} \tag{27}$$

$$\begin{aligned} & V_{s,t}^{\mathrm{EL,H_2}} + V_{s,t}^{\mathrm{H_2ST,H_2,d}} = V_{s,t}^{\mathrm{MR,H_2}} \\ & + V_{s,t}^{\mathrm{HFC,H_2}} + V_{s,t}^{\mathrm{HST,H_2,c}} \end{aligned} \tag{28}$$

$$\underline{p}^{\mathrm{e,grid}} \le p_{s,t}^{\mathrm{buy}} \le \overline{p}^{\mathrm{e,grid}} \tag{29}$$

$$\underline{V}^{\mathrm{g,grid}} \le V_{s,t}^{\mathrm{buy,g}} \le \overline{V}^{\mathrm{g,grid}} \tag{30}$$

where, $p_{s,t}^{\mathrm{buy}}$ and $V_{s,t}^{\mathrm{buy,g}}$ are the electricity purchased from the power grid and the gas purchased from the natural gas grid by the system at time t respectively; $h_{s,t}^{\mathrm{HST,c}}$ and $h_{s,t}^{\mathrm{HST,d}}$ are the heat storage power and heat release power of HST respectively; $V_{s,t}^{\mathrm{GST,g,c}}$ and $V_{s,t}^{\mathrm{GST,g,d}}$ are the gas storage capacity and gas release capacity of GST respectively; $V_{s,t}^{\mathrm{HST,H_2,c}}$ and $V_{s,t}^{\mathrm{H_2ST,H_2,d}}$ are the hydrogen storage capacity and hydrogen release capacity of H_2ST respectively; $\overline{p}^{\mathrm{e,grid}}$ and $\underline{p}^{\mathrm{e,grid}}$ are the upper and lower limits of the electricity purchased by the system respectively; $\overline{V}^{\mathrm{g,grid}}$ and $\underline{V}^{\mathrm{g,grid}}$ are the upper and lower limits of the natural gas purchased by the system respectively.

2.3 Objective function

A stochastic optimization model quantifies uncertainties in PV and WT output and in electrical, thermal and natural-gas loads. The objective is to minimize expected total operating cost, yielding the optimal resource-dispatch strategy:

$$\min \sum_{s=1}^{S} \left(c_s^{\mathrm{buy}} + c_s^{\mathrm{pv\&wt}} + c_s^{\mathrm{co_2}} \right) \tag{31}$$

where c_s^{buy} denotes the cost of purchasing electricity and natural gas, $c_s^{\mathrm{pv\&wt}}$ the penalty cost of renewable curtailment, and $c_s^{\mathrm{co_2}}$ the carbon trading cost. The analytical expressions of these three cost components are provided in Eqs. (30)–(32).

$$c_s^{\mathrm{buy}} = \sum_{t=1}^{T} \left(p_{s,t}^{\mathrm{buy}} \lambda_t^{\mathrm{e,buy}} + V_{s,t}^{\mathrm{buy,g}} \lambda_t^{\mathrm{g,buy}} \right) \tag{32}$$

$$c_s^{\mathrm{pv\&wt}} = \sum_{t=1}^{T} \begin{bmatrix} \delta^{\mathrm{PV}} \left(\overline{p}_{s,t}^{\mathrm{PV}} - p_{s,t}^{\mathrm{PV}} \right) + \\ \delta^{\mathrm{WT}} \left(\overline{p}_{s,t}^{\mathrm{WT}} - p_{s,t}^{\mathrm{WT}} \right) \end{bmatrix} \tag{33}$$

$$c_s^{\mathrm{co2}} = \sum_{t=1}^{T} \begin{pmatrix} a_1 p_{s,t}^{\mathrm{buy}} + a_2 p_{s,t}^{\mathrm{CHP}} \\ + a_3 h_{s,t}^{\mathrm{GB}} + a_4 h_{s,t}^{\mathrm{CHP}} \\ - a_5 V_{s,t}^{\mathrm{MR,gas}} \beta^{\mathrm{gas}} \end{pmatrix} \theta^{\mathrm{co_2}} \tag{34}$$

where, $\lambda_t^{\mathrm{e,buy}}$ and $\lambda_t^{\mathrm{g,buy}}$ are the electricity purchase price and gas purchase price at time t respectively; δ^{PV} and δ^{WT} are the penalty factors for abandoning solar

power and wind power respectively; a_{1-5} is the carbon emission factor of each resource; and θ^{co_2} is the carbon trading price.

3 Data and parameter settings

This section lists all case-study parameters. Rated capacities: electrolyzer 500 kW, MR 250 kW, HFC 250 kW, GB 800 kW, CHP 600 kW; corresponding efficiencies: 88 %, 60 %, 85 %, 95 %, 92 %. Each unit's ramp rate is limited to 50 % of rated capacity. Storage ratings: ESS 450 kW, HST 500 kW, GST 250 kW, H_2ST 200 kW; state-of-energy is bounded between 10 % and 90 % of capacity, charge/discharge power is capped at 50 % of rated power, and initial energy is 30 % of capacity. Curtailment penalties for PV and WT are 0.2. Carbon emission factors are 1.08, 0.23, 0.23, 0.39, 1, and the carbon price is 0.5 CNY/kg. Natural gas costs 2.76 CNY/m³. Time-of-use electricity prices: 0.46 CNY /kWh (01:00–07:00, 23:00–24:00), 0.82 CNY/kWh (08:00–11:00, 15:00–18:00), 1.44 CNY/kWh otherwise. Fifteen Monte Carlo scenarios for PV output, WT output, electricity, natural-gas, and heat demand are used. Please note that the energy pricing used in this study is based on actual price data for simulation experiments. By changing the input data, this IES framework can be applied to actual situations.

4 Results and discussion

Three cases evaluate the impacts of carbon trading and hydrogen equipment:

Case 1: the conventional architecture, which neither accounts for carbon trading nor incorporates any hydrogen devices (electrolyzer, MR, HFC and H_2ST).

Case 2: the conventional architecture augmented with carbon trading, yet still without hydrogen devices.

Case 3: the enhanced architecture that simultaneously introduces carbon trading and the four hydrogen devices.

All cases were solved on a laptop with an Intel Core i7-7700HQ @ 2.80 GHz using Python-Gurobi. Table 1 reports four key metrics for three scenarios. Case 1, the baseline, omits carbon trading and hydrogen equipment, yielding the highest mean solar- and wind-curtailment rates across fifteen Monte Carlo samples and the shortest runtime. Case 2 adds carbon trading: complexity and runtime rise, optimal system cost increases by 53.50 %, and curtailment drops by 21.17 % (solar) and 21.84 % (wind). Case 3 further integrates four hydrogen devices; complexity and runtime continue to increase, yet optimal cost falls by 28.85 % and curtailment decreases by an additional 11.66 % (solar) and 16.03 % (wind).

Table 1. Optimization results for different cases.

Projects	Case 1	Case 2	Case 3
Solution time (s)	1.20	1.59	10.17
Optimal total cost (CNY)	6163.84	9461.83	6732.27
Average solar abandonment rate (%)	35.89	14.72	3.06
Average wind abandonment rate (%)	40.01	18.17	2.14

Figs. 2–5 present the optimal dispatch of each resource in a representative Case 3 scenario. The schedules maintain strict power, heat, natural-gas and hydrogen balances at all times. The stochastic framework cuts operating cost and renewable curtailment while fully meeting electrical, thermal and natural-gas demands under uncertainties.

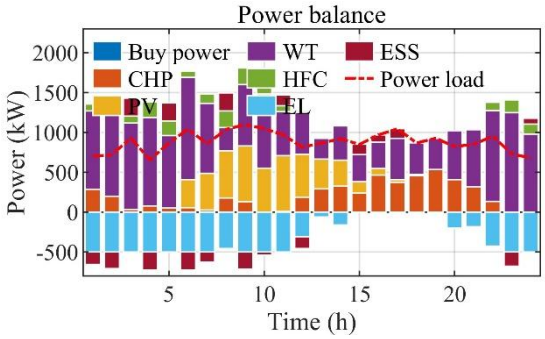

Fig. 2. Power balancing for the IES.

To quantify the effects of carbon price and hydrogen-related equipment on total system cost, we examined the optimal cost response to a carbon price increasing from 0 to 1 CNY/kg and to a simultaneous rise in MR efficiency—from 0.5 to 1.0 (MR denotes a representative hydrogen unit; analogous equipment behaves similarly). The results, depicted in Fig. 6, reveal that higher MR efficiency monotonically reduces total cost, whereas any increment in carbon price elevates it.

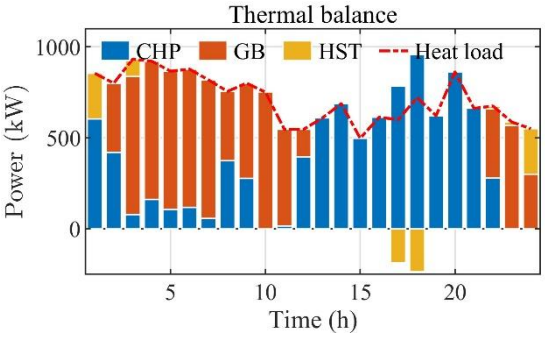

Fig. 3. Thermal balancing for the IES.

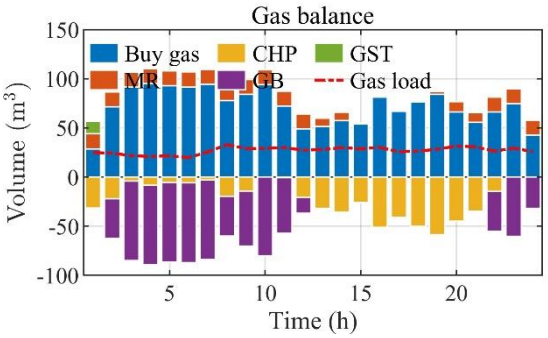

Fig. 4. Gas balancing for the IES.

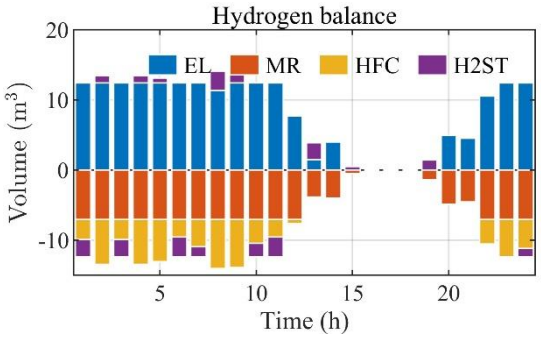

Fig. 5. Hydrogen balancing for the IES.

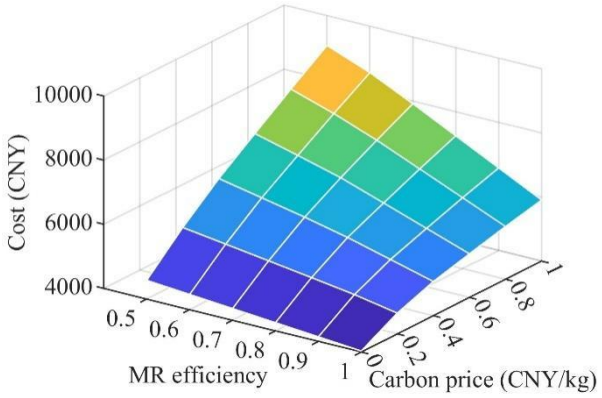

Fig. 6. The impact of carbon prices and MR efficiency on total cost

5 Conclusions

To meet deep-decarbonization targets, we propose a stochastic, electricity–heat–gas–hydrogen optimization framework that embeds a carbon-trading cost mechanism. The model co-optimizes four storage technologies—ESS, HST, GST, H_2ST—and three hydrogen devices: electrolyzer, HFC, and methanation reactor. Monte-Carlo-generated typical-day simulations yield:

1. Case 2 (carbon trading only): solution time is unchanged; operating cost rises 53.50 %; solar and wind curtailment falls to 21.17 % and 21.84 %, respectively.

2. Case 3 (carbon trading + hydrogen): runtime increases 6.4-fold; operating cost falls 28.85 %; curtailment drops to 3.06 % and 2.14 %.

Within acceptable computational limits, the hydrogen chain flexibly reduces both cost and curtailment, providing actionable guidance for low-carbon, high-renewable energy-system planning.

Credit Author Statement

Qiang Li: Conceptualization, Methodology, Software, Validation, Formal analysis, Writing - Original Draft, Writing - Review & Editing.
Zhonghao Wang: Data curation, Writing - Review & Editing.
Bo Jiang: Data curation, Writing - Review & Editing.
Fuxiang Dong: Data curation, Writing - Review & Editing.
Jinfu Liu: Supervision.
Peigang Yan: Supervision.
Daren Yu: Supervision.

Declaration of Competing Interest

The authors declare that they have no known competing financial interests or personal relationships that could have appeared to influence the work reported in this paper.

Data Availability

Data will be made available on request.

References

1. Li, Q., F. Wei, Y. Zhou, J. Li, G. Zhou, Z. Wang, J. Liu, P. Yan and D. Yu, A scheduling framework for VPP considering multiple uncertainties and flexible resources. Energy. 282, 20 (2023). https://doi.org/10.1016/j.energy.2023.128385
2. Li, Q., F. Dong, G. Zhou, C. Mu, Z. Wang, J. Liu, P. Yan and D. Yu, Co-optimization of virtual power plants and distribution grids: Emphasizing flexible resource aggregation and battery capacity degradation. Appl. Energy. 377, (2025). https://doi.org/10.1016/j.apenergy.2024.124519
3. Li, Q., Y. Zhou, F. Wei, S. Li, Z. Wang, J. Li, G. Zhou, J. Liu, P. Yan and D. Yu, Multi-time scale scheduling for virtual power plants: Integrating the flexibility of power generation and multi-user loads while considering the capacity degradation of energy storage systems. Appl. Energy. 362, (2024). https://doi.org/10.1016/j.apenergy.2024.122980
4. Wang, Y., Y. Wang, Y. Huang, J. Yang, Y. Ma, H. Yu, M. Zeng, F. Zhang and Y. Zhang, Operation optimization of regional integrated energy system based on the modeling of electricity-thermal-natural gas network. Appl. Energy. 251, (2019). https://doi.org/10.1016/j.apenergy.2019.113410
5. Jing, Y., M. Liang, H. Wang, Z. Yang, G. Li, F.P.G. Marquez, J. Yang and Z. Chen, Optimal economic and low-carbon scheduling in integrated energy system considering multi-level thermal energy coupling and integrated demand response. Energy Conv. Econom. 6, 2 83-100 (2025). https://doi.org/10.1049/enc2.70009
6. Wu, Y., P. Jin and Q. Li, Research on regulation strategy of integrated energy system based on game theory and divide-and-conquer algorithm. Energy. 319, (2025). https://doi.org/10.1016/j.energy.2025.134860
7. Chen, H., B. Yang, Z. Wang, H. Huang, Y. Zheng and Y. Sun, Collaborative optimization of regional integrated energy system with multiple energy storage. Appl. Therm. Eng. 276, (2025).

https://doi.org/10.1016/j.applthermaleng.2025.126969

8. Zhu, M., J. Fang, X. Ai, S. Cui, Z. Zhong and J. Wen, Real-Time Energy Management of Hydrogen Energy Hub-Based Industrial Integrated Energy Distribution System. IEEE Trans. Ind. Appl. 61, 1 1779-1789 (2025). https://doi.org/10.1109/tia.2024.3462698
9. Xu, X., B. Wang, M. Shi, G. Li, Y. Zhang, Q. Wang and D. Liu, Research on hydrogen storage system configuration and optimization in regional integrated energy systems considering electric-gas-heat-hydrogen integrated demand response. Int. J. Hydrog. Energy. 135, 86-103 (2025). https://doi.org/10.1016/j.ijhydene.2025.04.512
10. Liu, Z.-F., Y.-Y. Liu, H.-J. Jia, X.-L. Jin, T.-H. Liu and Y.-Z. Wu, Bi-level energy co-optimization of regional integrated energy system with electric vehicle to generalized-energy conversion framework and flexible hydrogen-blended gas strategy. Appl. Energy. 390, (2025). https://doi.org/10.1016/j.apenergy.2025.125868